Applied Catalysis B: Environmental 334 (2023) 122802

Contents lists available at ScienceDirect

Applied Catalysis B: Environmental

journal homepage: www.elsevier.com/locate/apcatb

Deep oxidation of toluene via combining a bifunctional catalyst with VUV photolysis

Shengjun Ye [a], Xiaoying Lian [a], Biyuan Liu [a], Haibao Huang [a,*], Boge Zhang [a], Zhuofeng Hu [a], Xianliang Fu [b], Guangqin Li [c], Zhenpan Zhang [a]

[a] School of Environmental Science and Engineering, Sun Yat-sen University, Guangzhou, China
[b] School of Materials Science and Engineering, Wuhan Institute of Technology, Wuhan, China
[c] School of Chemistry, Sun Yat-sen University, Guangzhou, China

ARTICLE INFO

Keywords:
VOCs
Catalytic oxidation
VUV photolysis
Bifunctional catalyst
O_3 utilization

ABSTRACT

Vacuum ultraviolet (VUV) photolysis presents a simple and promising method for volatile organic compounds (VOCs) degradation, while the formation of abundant organic and O_3 byproducts greatly limits its wide application. In this study, a bifunctional Mn/TiO_2-VM catalyst was developed and combined with VUV photolysis to promote VOCs deep oxidation via simultaneously enhancing its 254 nm UV ($h\nu_{254}$) and O_3 utilization. Compared with VUV photolysis alone, VUV photolysis well cooperated with catalytic oxidation for deep toluene degradation. In addition, most of O_3 byproduct was catalytically used for further deep oxidation of organic intermediates, greatly mitigating secondary pollution. The ability of strong electron transformation and O_3 utilization on bifunctional Mn/TiO_2-VM greatly enhance the generation of reactive oxygen species (ROS, ·OH and $\cdot O_2^-$), which accelerate the catalytic oxidation performance. This study originally demonstrates a deep VOCs oxidation strategy via VUV photolysis-catalytic synergy and greatly promoted the deep understanding and application of VUV technology.

1. Introduction

Volatile organic compounds (VOCs) are the major air pollutants and cause great hazards to the environment and human health [1]. It is estimated that anthropogenic VOCs emission in China reached 25.9 million tons in 2020 and was still increasing [2,3]. Benzene, toluene, ethylbenzene, and xylene (BTEX) accounting for 43% of total anthropogenic VOCs emission [4–6] have strong photochemical activity and toxicity and should be deeply removed [2]. Many methods including thermal burning [7], catalytic combustion [7], absorption [8] and condensation [9] have been developed to remove high-concentration VOCs. As for low-concentration VOCs, some strategies such as plasma catalysis [10], photocatalysis [11,12], and ozone (O_3) catalytic oxidation [13] have been intensively studied due to the simplicity and mild conditions, however, their application is still significantly limited by low efficiency and abundant byproducts. Therefore, it is urgent to develop efficient and deep oxidation processes for low-concentration VOCs waste gas at mild conditions.

In the last two decades, vacuum ultraviolet (VUV) photolysis has attracted increasing attention in removing VOCs, NO_x and SO_2 due to its advantages of simplicity and low cost [14,15]. The VUV lamp can concurrently produce UV light of about 10% 185 nm ($h\nu_{185}$) and 90% 254 nm ($h\nu_{254}$) [14,16,17]. The high-energy photon of $h\nu_{185}$ can directly destruct VOCs, and dissociate oxygen (O_2) and water (H_2O) molecular to form hydroxyl radicals (·OH), superoxide radicals ($\cdot O_2^-$), O_3 and other reactive species (Eqs. 1–6) [14,17,18] for VOCs degradation [19], nevertheless, the energy of $h\nu_{254}$ is not well utilized. In addition, massive organic and O_3 byproducts are generated during VUV photolysis of VOCs [18], which dramatically limits its wide application. Hence, the efficient utilization of O_3 and $h\nu_{254}$ in VUV photolysis is highly required for boosting deep oxidation of VOCs and avoiding the emission of toxic byproducts and energy loss.

1.1. Gas-phase reactions in the VUV system

$$h\nu_{185} + H_2O \rightarrow \cdot OH + \cdot H \quad (1)$$

* Corresponding author.
E-mail address: seabao8@gmail.com (H. Huang).

https://doi.org/10.1016/j.apcatb.2023.122802
Received 7 February 2023; Received in revised form 3 April 2023; Accepted 22 April 2023
Available online 23 April 2023

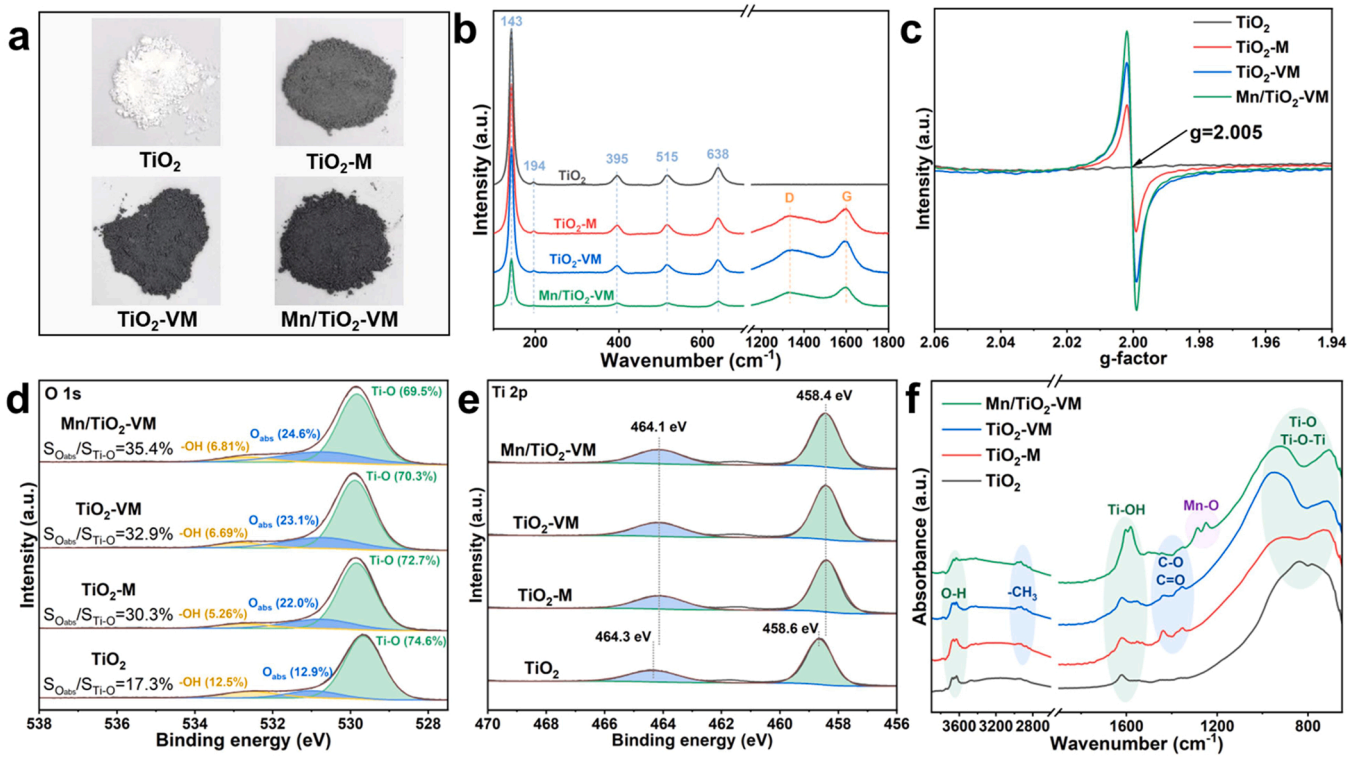

Fig. 1. The colors (a), Raman spectra (b), solid EPR spectra(c), and high-resolution XPS spectra of O 1 s (d) and Ti 2p (e), and FTIR spectra (f) of TiO_2, TiO_2-M, TiO_2-VM and Mn/TiO_2-VM samples.

$$h\nu_{185} + O_2 \rightarrow O(^1D) + O(^3P) \quad (2)$$

$$O(^3P) + O_2 \rightarrow O_3 \quad (3)$$

$$O_3 + h\nu_{254} \rightarrow O(^1D) + O_2 \quad (4)$$

$$O_3 + H_2O + O(^1D) \rightarrow 2{\cdot}O_2^- + 2\,H^+ \quad (5)$$

$$O(^1D) + H_2O \rightarrow 2{\cdot}OH \quad (6)$$

To utilize $h\nu_{254}$ of VUV irradiation, TiO_2 photocatalyst was combined to construct VUV photocatalytic oxidation systems [20–22]. VUV photocatalytic oxidation can sustain high photocatalytic activity and long-term stability since the active species in the gas-phase can effectively reduce the accumulation of intermediates on the catalyst surface [18,20,23]. However, the limited O_3 removal capacity of TiO_2 resulted in numerous residues and low utilization of O_3. Although the O_3 utilization has been improved by coupling O_3 catalysts (such as MnO_x/ZSM-5) and composite catalysts (such as Mn/TiO_2/ZSM-5) [16–18,22,24], the limited photocatalytic activity still cannot achieve high $h\nu_{254}$ utilization. It still presents a great challenge to concurrently enable efficient utilization of $h\nu_{254}$ and O_3 for deep VOCs degradation.

In this study, a bifunctional Mn/TiO_2-VM catalyst with plentiful carbon (C), oxygen vacancy (O_v) and Mn active sites was originally developed for VUV photolysis to achieve efficient VOCs oxidation via simultaneously enhancing $h\nu_{254}$ and O_3 utilization. The obtained novel VUV catalytic oxidation process was used to eliminate toluene, a typical aromatic VOC, in the continuous flow reactor. DFT calculation, time-resolved FTIR and PTR-TOF-MS were investigated to explore the mechanisms of the VUV catalytic oxidation system. Based on the above research and analysis, we aimed at maximizing the energy utilization of the VUV system, achieving deep VOCs disposal and green emissions, and analyzing the internal complex mechanisms. To the best of our knowledge, this work presents the first example of boosting VUV catalytic oxidation of VOCs by combining multiple active sites, highlighting its potential for application in waste gas treatment.

2. Material and methods

2.1. Preparation of catalysts

TiO_2-M, TiO_2-VM and Mn/TiO_2-VM were prepared by surface treatments of commercial TiO_2 (P25, Degussa, Germany). In the naming of the samples, "V" refers to the surface treatment on VUV irradiation, and "M" refers to the surface treatment on methanol. Detailed methods for preparation and naming of catalysts were elaborated in Supporting Information.

2.2. Toluene catalytic degradation measurements

As shown in Fig. S2, catalytic degradation of toluene was conducted in a continuous-flow VUV catalytic oxidation system, which consisted of a quartz tube photolysis module with a VUV lamp (ZW4D15Y-Z212, COMWIN, China) and a cuboid shaped catalytic reaction module. $h\nu_{254}$ from the VUV lamp was transmitted to the catalysts in the catalytic reaction module. 1 L/min air flowed with 20 ppm toluene was generated from the gas distribution system and then introduced into the VUV catalytic oxidation system. Toluene was firstly degraded in the VUV photolysis module, and the residual organic pollutants and O_3 were introduced into the catalytic reaction module for further oxidation under the help of catalysts and $h\nu_{254}$ irradiation. The residence time of gas in the quartz tube and the catalytic reaction module were 1 s and 9 s, respectively. Toluene and CO_2 were detected by the gas chromatography (GC9790Plus, China) and O_3 was analyzed by O_3 analyzer (49i, Thermo Fisher, USA). Calculation methods of toluene, CO_2 and O_3 were shown in Supporting Information.

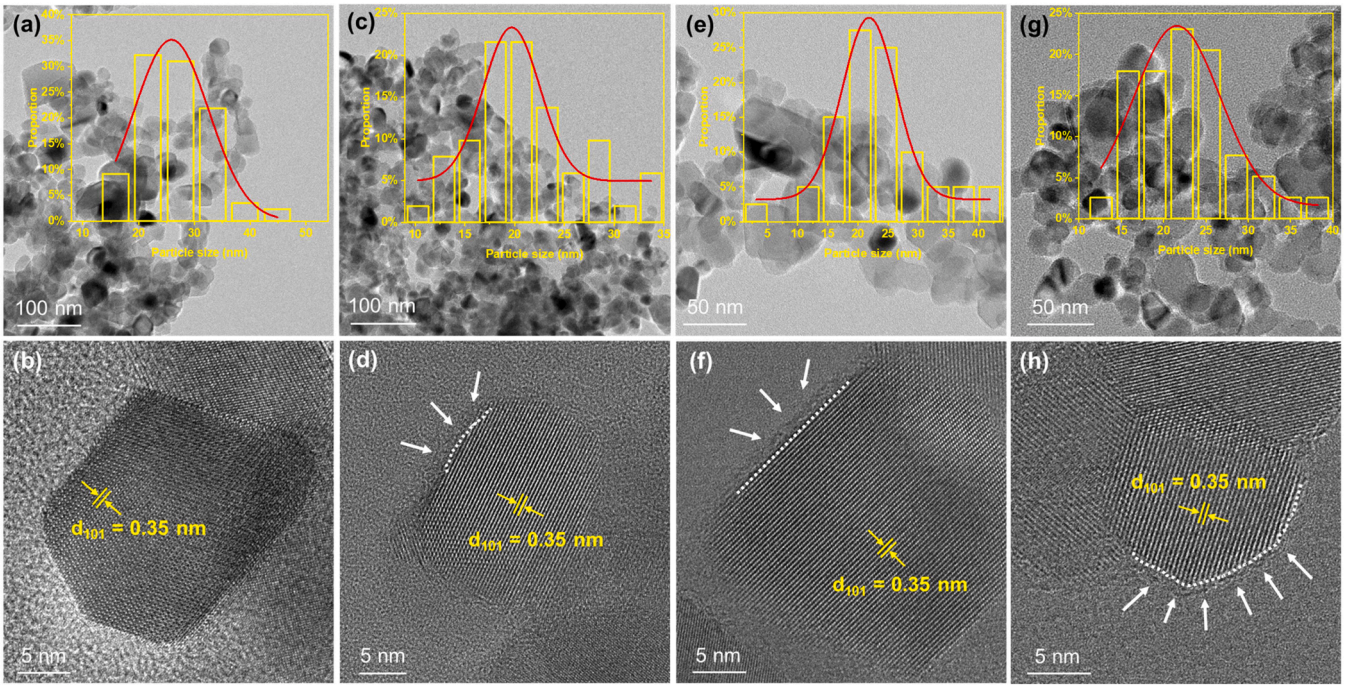

Fig. 2. TEM and HRTEM images of TiO_2 (a, b), TiO_2-M (c, d), TiO_2-VM (e, f) and Mn/TiO_2-VM (g, h).

2.3. Toluene degradation mechanism

Time-resolved in situ DRIFTS experiments were conducted on a Nicolet iS10 FTIR spectrometer (Thermo Fisher, USA). All samples were pretreated with air at 100 °C for 30 min to remove impurities adsorbed on the surface, and the samples were purged with N_2 and cooled to 25 °C. After the pretreatment, the toluene mixture (50% relative humidity) was passed into the reaction chamber and kept in the dark environment for 30 min. Subsequently, the VUV lamp was turned on to start irradiation for 60 min. The toluene degradation byproducts were identified by proton-transfer-reaction time-of-flight mass spectrometry (PTR-TOF-MS, Ionicon Analytik GmbH, Innsbruck, Austria).

3. Results and discussion

3.1. Structural and optical properties

Catalysts were characterized to realize the structural properties. As shown in Fig. 1a, the colors of TiO_2 changed to grayish-blue over TiO_2-M and grayish-black over TiO_2-VM and Mn/TiO_2-VM after surface treatments. All samples showed similar Raman spectra (Fig. 1b) and XRD patterns (Fig. S3) of TiO_2 [25], revealing that the crystal phases of TiO_2 were not changed after the surface treatments. No relevant XRD peaks of manganese oxides were found on Mn/TiO_2-VM due to low Mn doping. As shown in TEM (Fig. 2) and BET results (Fig. S4), the particle sizes, the specific surface area and pore sizes of TiO_2 also did not change significantly after surface treatments. However, the Raman peaks intensities of various TiO_2 samples were gradually weakened with the order of TiO_2 > TiO_2-M > TiO_2-VM > Mn/TiO_2-VM (Fig. S5), proving that the surface lattice disorder of TiO_2 was greatly enhanced after surface treatments. In particular, the VUV irradiation and Mn doping together could result in significant surface defects of TiO_2 lattice over Mn/TiO_2-VM. Additionally, the D band (1330 cm^{-1}) and G band (1594 cm^{-1}) appeared on all the surface-treated TiO_2 samples (Fig. 1b). Typically, the D and G bands represent the defects in the lattice and in-plane stretching vibration of the sp^2 hybridization of carbon atoms, respectively [26], proving the existence of graphitic carbon layers, which were derived from the carbonization of CH_3OH after surface treatment. In HRTEM images (Fig. 2), the treated samples showed a disordered shell, which well agreed with the Raman results. Hence, obvious lattice disordering and graphitic carbon were successfully formed on the Mn/TiO_2-VM after surface treatments.

The EPR spectra were used to illustrate the presence of oxygen vacancies (O_v). As shown in Fig. 1c, TiO_2-M, TiO_2-VM and Mn/TiO_2-VM showed strong amplitudes at g = 2.005 in EPR spectra, while no signal could be found in original TiO_2, suggesting the formation of O_v after the surface treatments [27,28]. In particular, Mn/TiO_2-VM exhibited the strongest O_v signal. This was due to the joint promotion of VUV irradiation and Mn doping on the reduction effect of methanol on TiO_2, and stronger reduction effect led to the formation of more O_v on TiO_2 surface. XPS analysis was conducted to further confirm the existence of O_v on treated samples (Fig. 1d, e). The O 1 s XPS signals could be divided into three peaks at 529.8, 531.2, and 532.6 eV (Fig. 1d), which were ascribed to surface lattice oxygen of Ti−O, absorbed oxygen (O_{abs}) and absorbed water (−OH), respectively [27]. Previous studies have shown that O_v can increase the peak area ratios of O_{abs} and Ti−O ($S_{Oabs}/S_{Ti\text{-}O}$) [29,30]. The $S_{Oabs}/S_{Ti\text{-}O}$ were estimated to be 17.3%, 30.3%, 32.9% and 35.4% in TiO_2, TiO_2-M, TiO_2-VM, and Mn/TiO_2-VM, respectively, indicating the increase of O_v after the surface treatments [28]. The very weak peaks of Mn 2p and Mn 3s on Mn/TiO_2-VM were detected (Fig. S6), owing to its low Mn content [31–33]. It was found that the Mn element on the surface of Mn/TiO_2-VM mainly existed in the form of + 3 and + 4 valences, and the average oxidation state (AOS) was 3.45 [31–33]. Compared with TiO_2, Ti $2p_{3/2}$ and Ti $2p_{1/2}$ peaks negatively shifted from 458.6 eV and 464.3 eV to 458.4 eV and 464.1 eV for TiO_2-M, TiO_2-VM and Mn/TiO_2-VM (Fig. 1e), respectively, indicating the partial transfer of Ti^{4+} to Ti^{3+} due to the presence of O_v [28,34]. Hence, the solid EPR and XPS results proved the existence of abundant O_v and a small amount of Mn on Mn/TiO_2-VM.

FTIR spectra can be used to analyze the surface functional groups of the samples. The results (Fig. 1f) showed that all the catalysts had characteristic peaks of hydroxyl groups (O−H in 3630 cm^{-1} and Ti−OH in the range of 1620–1552 cm^{-1}) [35–37]. In particular, the Ti−OH peak strength of Mn/TiO_2-VM was significantly increased, demonstrating more abundant −OH groups on the sample surface. Previous studies have shown that abundant surface hydroxyl groups on TiO_2 can

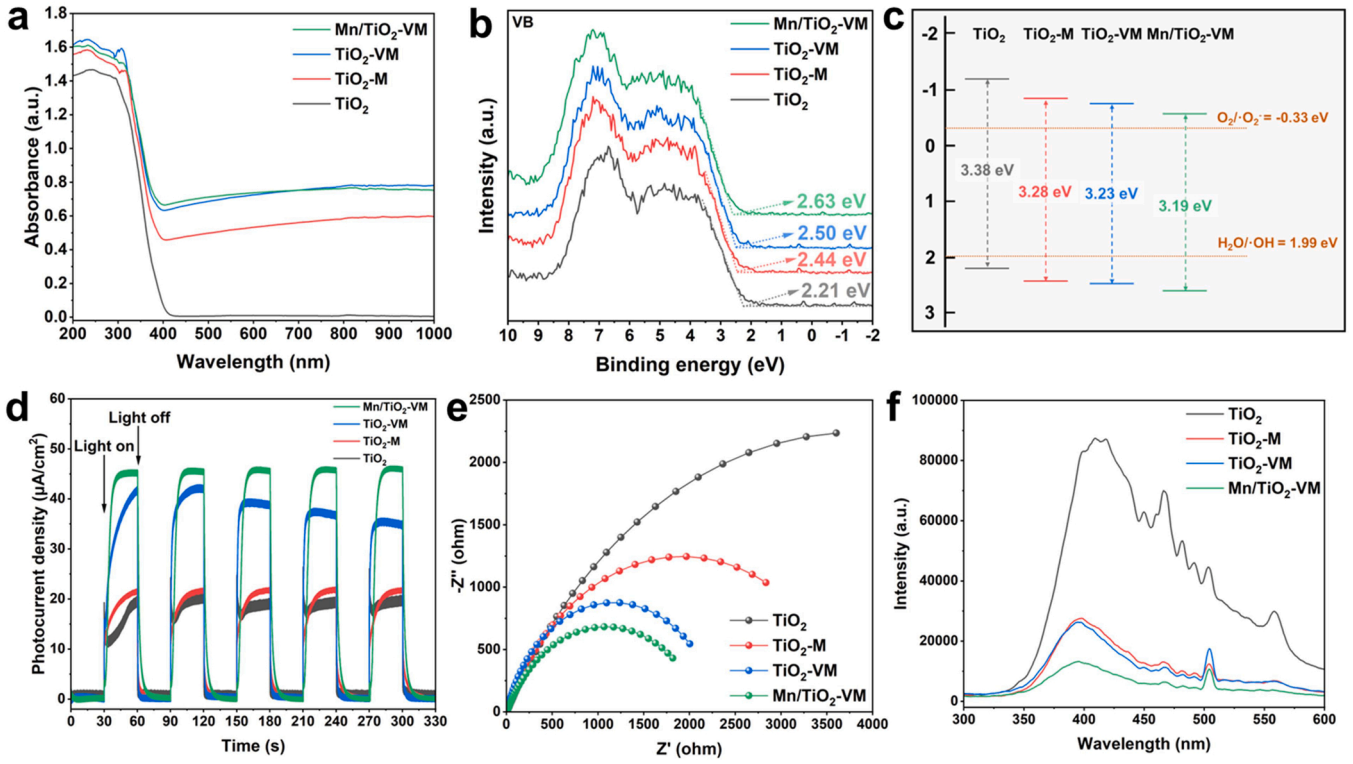

Fig. 3. UV-Vis DRS spectra (a), VB-XPS spectra (b), schematic diagram of VB-CB position (c), transient photocurrent (TPC) responses (d), electrochemical impedance (EIS) spectra (e) and steady state fluorescence (PL) spectra (the excitation wavelength is 250 nm) (f) of TiO_2, TiO_2-M, TiO_2-VM and Mn/TiO_2-VM samples.

significantly improve catalytic performance [38,39]. Therefore, the large number of Ti−OH structures on the surface of Mn/TiO_2-VM may also enhance the catalytic degradation of VOCs. The peaks in the range of 2964 − 2829 cm^{-1}, in 1439 cm^{-1} and 1354 cm^{-1} of treated samples corresponded to $-CH_3$, C═O and C−O [37], respectively, which were due to CH_3OH treatments. Additional peaks appeared at 1288 cm^{-1} and 1251 cm^{-1} on Mn/TiO_2-VM, which were most likely ascribed to the formation of Mn−O structure after Mn doping. Moreover, the characteristic peaks of TiO_2 near 800 cm^{-1} (Ti−O−Ti and Ti−O) were shifted after surface treatments, showing the changes in chemical bond energy and force constants on catalyst surfaces [40]. The lowest H_2-TPR temperature of Mn/TiO_2-VM (473 °C, Fig. S7) revealed that Mn/TiO_2-VM had the most active redox activity [41,42], proving that the surface chemical bond energy and force constant characteristics of Mn/TiO_2-VM were conducive to the enhancement of its redox capacity. Therefore, the Raman spectra, solid EPR, XPS, HRTEM, FTIR and H_2-TPR results clearly demonstrated the formation of multiple C, O_v and Mn surface sites and the strong surface redox property over Mn/TiO_2-VM after the surface treatment process.

The optical properties and photogenerated mobility of the catalyst samples were further investigated. The photoabsorption was analyzed by UV-Vis DRS spectra, as shown in Fig. 3a. All samples had strong absorption in the UV region with an absorption edge of approximately 400 nm, indicating that they could be efficiently activated by $h\nu_{254}$ [38]. Based on the UV-Vis DRS spectra, the bandgaps of the samples (Fig. S8) were estimated through the plot of $(\alpha h\nu)^n$ vs $h\nu$ from the Tauc equation (Eq. (S4) in Text S6). The bandgaps of TiO_2 and Mn/TiO_2-VM were 3.38 and 3.19 eV, respectively, allowing the electrons (e^-) to be excited at lower photon energies on Mn/TiO_2-VM. The narrower bandgap led to the formation of more photogenerated carriers for photocatalytic oxidation [43]. The VB-XPS results (Fig. 3b) revealed the VB positions of TiO_2 (2.21 eV), TiO_2-M (2.44 eV), TiO_2-VM (2.50 eV) and Mn/TiO_2-VM (2.63 eV). Therefore, according to the formula $E_{CB} = E_{VB} - E_g$ and the VB-XPS results, the energy bands of all samples was illustrated in Fig. 3c. Theoretically, all samples could convert H_2O and O_2 to ·OH and $\cdot O_2^-$ owing to their high VB (> 1.99 eV) and low CB (< −0.33 eV) [44,45], and Mn/TiO_2-VM showed the most active h^+ activity due to the lowest VB.

Since the transfer efficiency of photogenerated carriers plays an important role in catalytic reactions, transient photocurrent (TPC) responses, electrochemical impedance (EIS), and steady state fluorescence tests were investigated. The TPC responses revealed that the photoinduced electron density of these samples decreased in the order of Mn/TiO_2-VM > TiO_2-VM > TiO_2-M > TiO_2 (Fig. 3d). Consistently, Mn/TiO_2-VM showed the lowest electron transfer resistance in the EIS spectra (Fig. 3e). In addition, Mn/TiO_2-VM showed the lowest PL intensity (Fig. 3f). Hence, Mn/TiO_2-VM showed the highest charge generation and charge mobility, and lowest photogenerated carriers recombination, which were probably due to the increased surface sites of C, O_v and Mn [46]. Therefore, more e^- and photogenerated holes (h^+) could participate in the reaction with toluene and O_3 over Mn/TiO_2-VM.

3.2. *VUV catalytic toluene oxidation performance*

The catalytic performances of the samples were evaluated under the VUV catalytic oxidation process, as shown in Figs. 4 and S9. Toluene removal efficiency over various catalysts was increased with the order of 'No catalyst (50%) < TiO_2 (59%) < TiO_2-M (66%) < TiO_2-VM (70%) < Mn/TiO_2-VM (80%) (Figs. 4a and S9a). In Figs. 4b, c and S9b, c, mineralization rates and O_3 removal efficiencies also followed the same orders. The surface treated samples improved the degradation and mineralization rate of toluene, as well as the removal of O_3. In particular, Mn/TiO_2-VM showed the best catalytic performance in the VUV system. Compared with VUV photolysis, toluene degradation efficiency and mineralization rate were significantly increased by 30% and 42% over Mn/TiO_2-VM, while only 9% and 17% over TiO_2, respectively (Fig. 4a and b). The catalytic degradation and mineralization performance of Mn/TiO_2-VM were 3.3 times and 2.5 times higher than that of

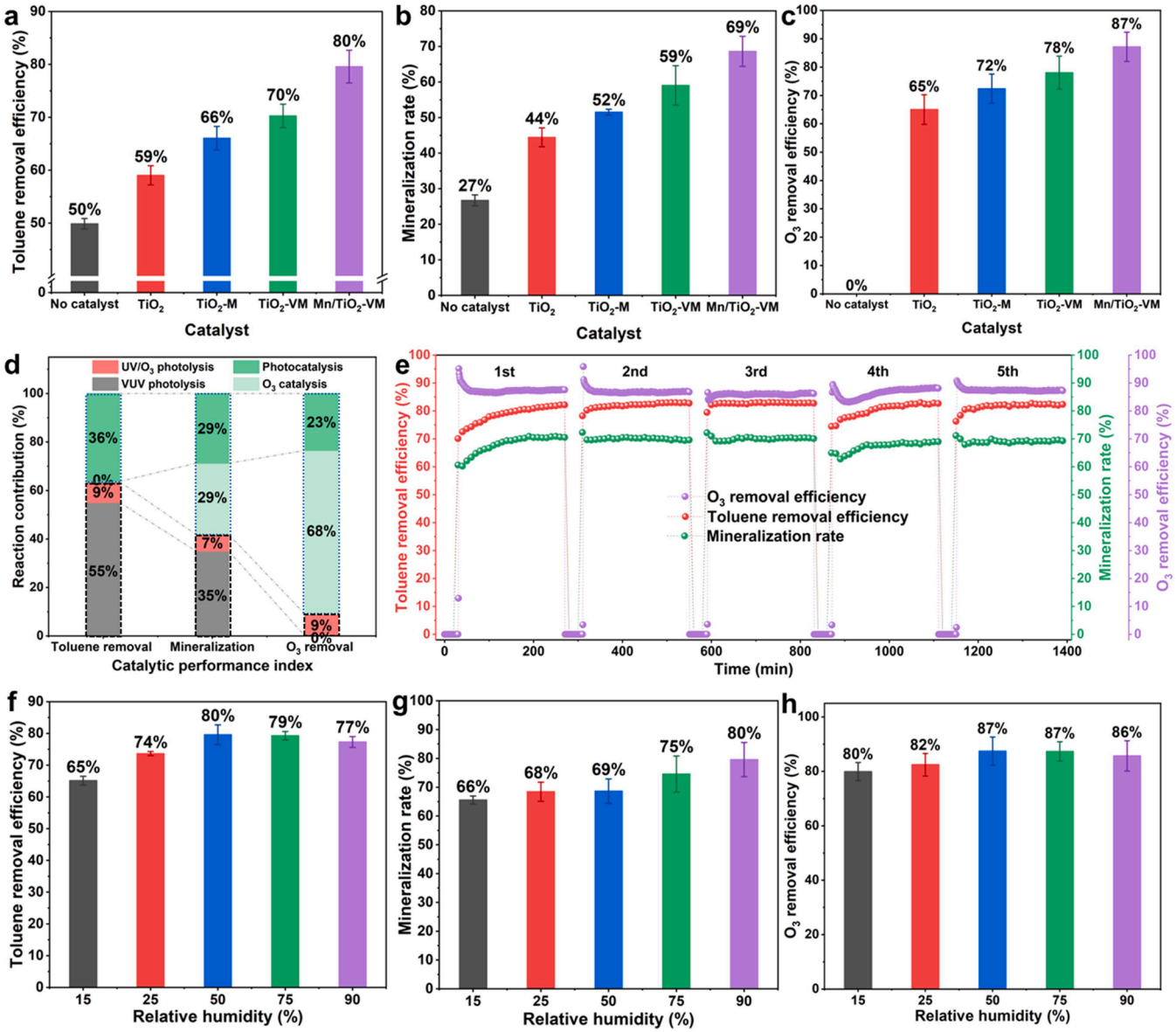

Fig. 4. Toluene removal efficiency (a), mineralization rate (b) and O_3 removal efficiency (c) on TiO_2, TiO_2-M, TiO_2-VM and Mn/TiO_2-VM samples under VUV irradiation for 240 min at 50% relative humidity. Contribution of each reaction process to toluene removal, mineralization rate and O_3 removal (d) (The black dashed rectangles represent the contribution of gas-phase reaction, and the blue dashed rectangles represent the contribution of catalyst interface reaction; gas-phase reaction = VUV photolysis + UV/O_3 photolysis; catalytic oxidation = O_3 catalysis + photocatalysis). Long-term stability test for Mn/TiO_2-VM at 50% relative humidity (e). Toluene removal efficiency (f), mineralization rate (g) and O_3 removal efficiency (h) in different relative humidity on Mn/TiO_2-VM samples under VUV irradiation for 240 min.

TiO_2, proving the significant enhancement of catalytic oxidation activity after the surface treatment. Furthermore, abundant O_3 of more than 60 ppm was generated from VUV irradiation (Fig. S9c). However, the O_3 removal efficiency of Mn/TiO_2-VM could be stably maintained above 86% and was also the highest (Fig. S9c). Hence, it could be concluded that Mn/TiO_2-VM showed the greatest removal performance of both toluene and O_3, indicating that toluene degradation and mineralization were closely related to O_3 elimination and utilization in VUV system. Based on the above analysis, it could be inferred that the cooperation of C, O_v and Mn sites on Mn/TiO_2-VM might greatly enhance the ability to utilize hν_{254} and O_3, and promote the separation of e^- and h^+ on TiO_2, which may be conducive to the redox reaction of pollutants on the catalyst surface.

Due to the co-existence of hν_{254}, hν_{185}, O_3 and catalysts in the VUV catalytic oxidation system, toluene degradation is very complex, including oxidation reactions in the gas-phase and at the catalyst interface. VUV photolysis and UV/O_3 photolysis mainly happened in the gas-phase. Catalytic degradation of toluene was mainly ascribed to O_3 catalytic and photocatalytic oxidation at the catalyst interface. Hence, toluene degradation experiments were carried out with and without the hν_{254} irradiation and the Mn/TiO_2-VM in the catalytic oxidation module to clarify the contribution of different reaction processes (i.e., VUV photolysis, UV/O_3 photolysis, O_3 catalysis and photocatalysis) to toluene degradation, mineralization and O_3 removal. Detailed operating conditions and calculation method can be seen in Supporting Information (Fig. S10). The reaction sub-processes under different operating conditions were shown in Table S1 and Fig. S10. As can be seen from Fig. S11, toluene degradation efficiencies, mineralization rates and O_3 removal efficiencies were totally different under different operating conditions. The normalized contribution of different reaction processes could be obtained through calculation (the detailed calculation process can be seen in the Supporting Information in Text S7) and the results

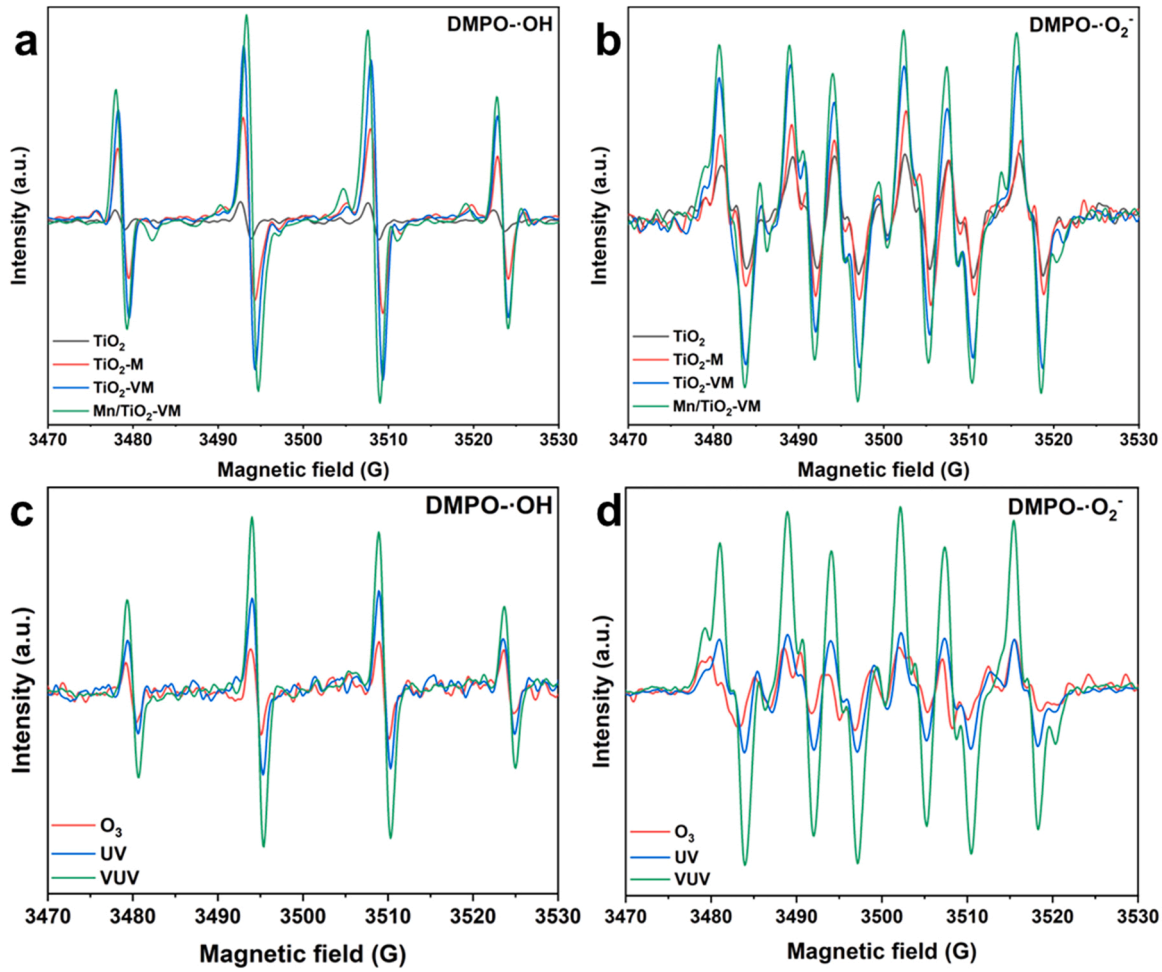

Fig. 5. EPR spectra of ·OH (a) and·O_2^- (b) signals of TiO_2, TiO_2-M, TiO_2-VM and Mn/TiO_2-VM samples under VUV irradiation. EPR spectra of ·OH (c) and ·O_2^- (d) signals of Mn/TiO_2-VM samples under the condition of O_3 environment, UV irradiation and VUV irradiation.

were shown in Fig. 4d. 64% and 36% of removed toluene were attributed to degradation by gas-phase photolysis and catalytic oxidation, respectively. In particular, VUV photolysis account for 55% of toluene degradation and was the main sub-process in gas-phase. Catalytic oxidation of toluene was almost attributed to photocatalysis due to superior capacity for the generation and separation of photogenerated carriers (as illustrated in Fig. 4d), while O_3 catalysis nearly did not work on preliminary degradation of toluene. As for toluene mineralization, gas-phase photolysis contributed 42% (35% for VUV photolysis and 7% for UV/O_3 photolysis) and catalytic oxidation accounted for 58% (29% for O_3 catalysis and 29% for photocatalysis), demonstrating the significant role of catalytic oxidation in toluene mineralization. Although O_3 catalysis was not involved in the initial toluene degradation, it contributed to 29% mineralization of toluene since intermediate products of toluene could be oxidized by O_3 catalysis. Unlike the contribution of toluene removal, 91% O_3 removal was attributed to catalytic oxidation while only 9% to gas-phase photolysis, indicating that the catalytic process was mainly responsible for removing and utilizing O_3. According to the obtained results, the addition of Mn/TiO_2-VM greatly improved toluene removal and O_3 utilization in the VUV catalytic oxidation system, revealing that gas-phase photolysis and catalytic oxidation could cooperate well on toluene degradation and mineralization [47].

Moreover, the durability and adaptability of Mn/TiO_2-VM in VUV catalytic toluene oxidation system were also studied. In the 5 cyclic stability tests on Mn/TiO_2-VM (Fig. 4e), catalytic oxidation performance was kept highly stable after reaction for 1400 min, toluene removal efficiency, mineralization rate and O_3 removal efficiency maintained at about 82%, 70% and 90%, respectively. Also, the used Mn/TiO_2-VM sample was collected and analyzed by solid EPR and FTIR spectroscopy (Fig. S12). Solid EPR showed that the strength of O_v did not change significantly after reaction (Fig. S12a). Due to the accumulation of toluene byproducts on the surface, the FTIR spectrum of the used sample was quite different from that of the original sample (Fig. S12b), but the $-CH_3$ (2964–2829 cm^{-1}), C═O (1439 cm^{-1}), C−O (1354 cm^{-1}) and Mn−O (1288 cm^{-1} and 1251 cm^{-1}) structures on the surface still existed. It might be due to the structures of surface sites (C, O_v and Mn) that promote the stable and efficient removal of toluene and O_3 in VUV catalytic oxidation system. Additionally, toluene degradation was carried out in different relative humidity (Figs. 4f-h and S13). When the relative humidity was increased from 15% to 90%, toluene removal efficiency, toluene mineralization and O_3 removal efficiency were increased, reaching their max values of 80%, 80% and 87%, respectively. Among them, as the relative humidity increased, toluene degradation efficiency showed a trend of first increasing and then slightly decreasing. This was because an appropriate amount of water molecules in the air could promote the generation of ROS in the gas phase (Eqs. (1) and (5)) and on the catalyst surface. However, too many water molecules would occupy the active sites of the catalyst that caused the decrease of catalytic degradation. Toluene mineralization rate was significantly increasing with the increase of relative humidity, which might be due to the fact that a large number of water molecules were the good mediums for the reaction between organic substances and ROS, thereby enhancing the mineralization effect to some extent. And the relative humidity had little effect on O_3 removal efficiency. However, in

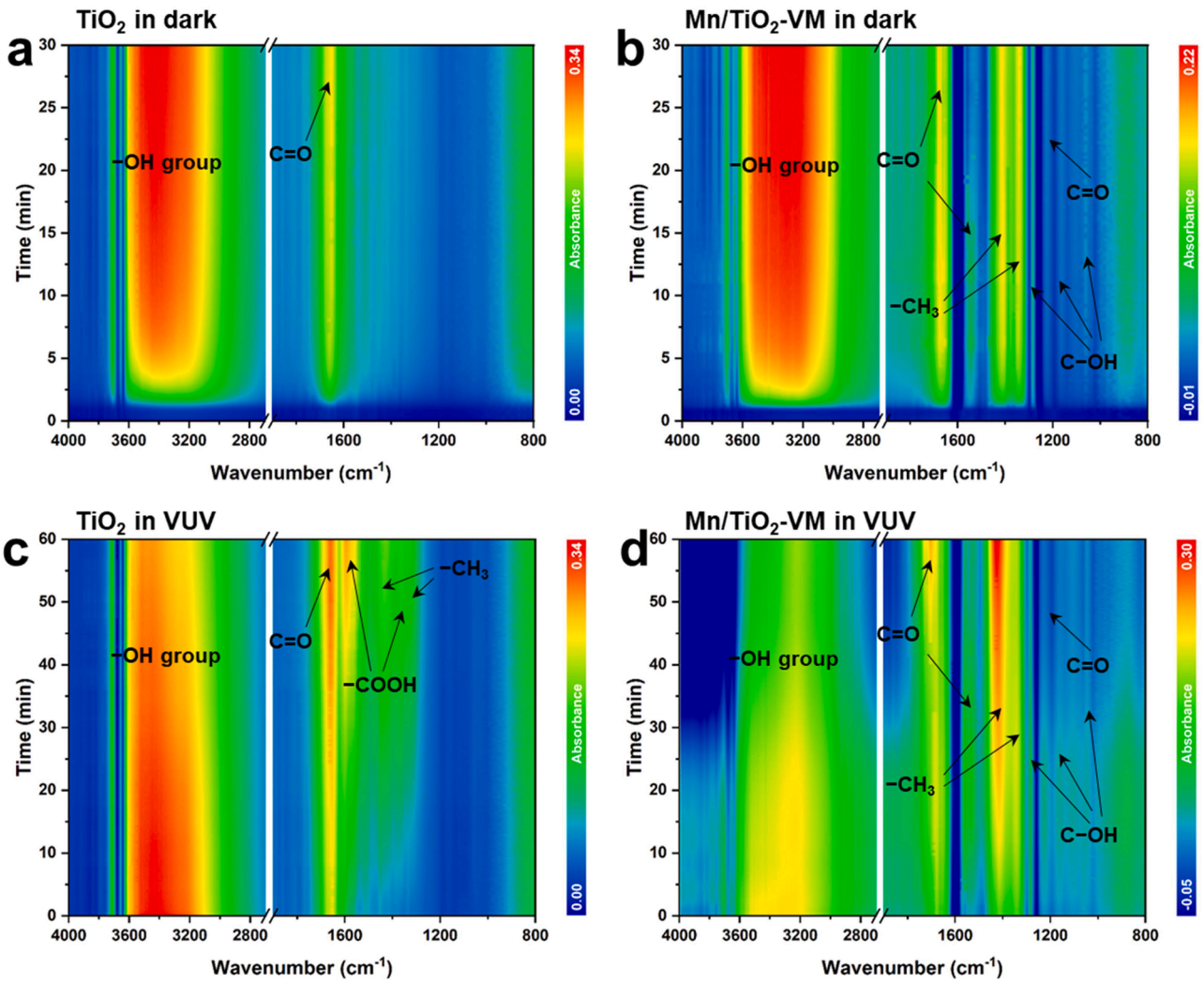

Fig. 6. Three-dimensional in-situ DRIFTS spectra on TiO_2 (a, c) and Mn/TiO_2-VM (b, d) samples in dark and under VUV irradiation.

general, the system could maintain good purification capacity under different humidity. Therefore, the system performed well in long-term running and different environmental humidity, indicating great durability and wide adaptability.

3.3. Mechanism study

According to the above results, the addition of Mn/TiO_2-VM greatly improved the photocatalytic oxidation and O_3 catalysis performance for toluene degradation and mineralization. It is necessary to deeply look insight into the cooperative promotion mechanisms and toluene degradation pathways. The density functional theory (DFT) calculation was carried out to figure out the key active sites. The adsorption energies (ΔE_{DFT}) and Bader charges of C and Mn elements on Mn/TiO_2-VM were shown in Table S4 and Fig. S14. According to the strength of ΔE_{DFT} (Table S4), H_2O was most easily adsorbed at the graphite C layer (−1.28 eV), O_3 was most easily adsorbed at the O_v site (−4.36 eV), and O_2 was also easily adsorbed at the O_v (−4.52 eV) and Mn sites (−3.42 eV). The results of Bader charges (Fig. S14) revealed that the C site on the graphite layer was the electron-rich region (0.21e), which helped to capture h^+ and H_2O. And the Mn site was the electron-deficient region (−0.96e), which could promote to capture e^- and O_3. In the meanwhile, abundant O_v sites on Mn/TiO_2-VM were also electron-deficient regions [27,28], which is beneficial to capture O_2, O_3 and e^-. Hence, DFT results clearly indicated that the multiple active sites of C, O_v and Mn could well cooperate together to efficiently adsorb and activate reactant species.

EPR was further used to identify the ROS during the catalytic oxidation reaction. The DMPO-·OH and DMPO-·O_2^- signals were detected over all samples (Fig. 5a, b) and no TEMP-$^1O_2$ signal was detected (Fig. S15). Obviously, Mn/TiO_2-VM showed the strongest signal strengths (Fig. 5a, b), proving that Mn/TiO_2-VM could generate most ·OH and ·O_2^- under VUV irradiation because of its best charge generation, transformation and separation on multiple active sites (Fig. 3d-f), which well explained the exceptional catalytic activity towards toluene degradation and mineralization. Moreover, catalytic generation of ROS over Mn/TiO_2-VM with the exposure of O_3, UV and VUV was studied to explore the synergistic effects of O_3 and $h\nu_{254}$ (Fig. 5c, d). Much more ·OH and ·O_2^- were produced in VUV irradiation than O_3 and $h\nu_{254}$ alone, indicating that O_3 catalysis and photocatalysis could synergistically promote the activation of H_2O, O_2 and O_3, thus improving the redox ability in the VUV catalytic oxidation system. The reason for the improved activating ability under VUV irradiation is that O_3 is a powerful e^- acceptor, and e^- is easily captured by O_3, which makes the quicker separation of photogenerated carriers on the surface of the catalyst. Additionally, O_3 catalysis itself can also generate ROS, which helps produce more ROS. The ERP results can be inferred that the VUV photolysis in gas-phase and ROS oxidation at the catalyst interface led to efficient degradation and high mineralization of toluene.

To further explore the toluene degradation processes at the catalyst

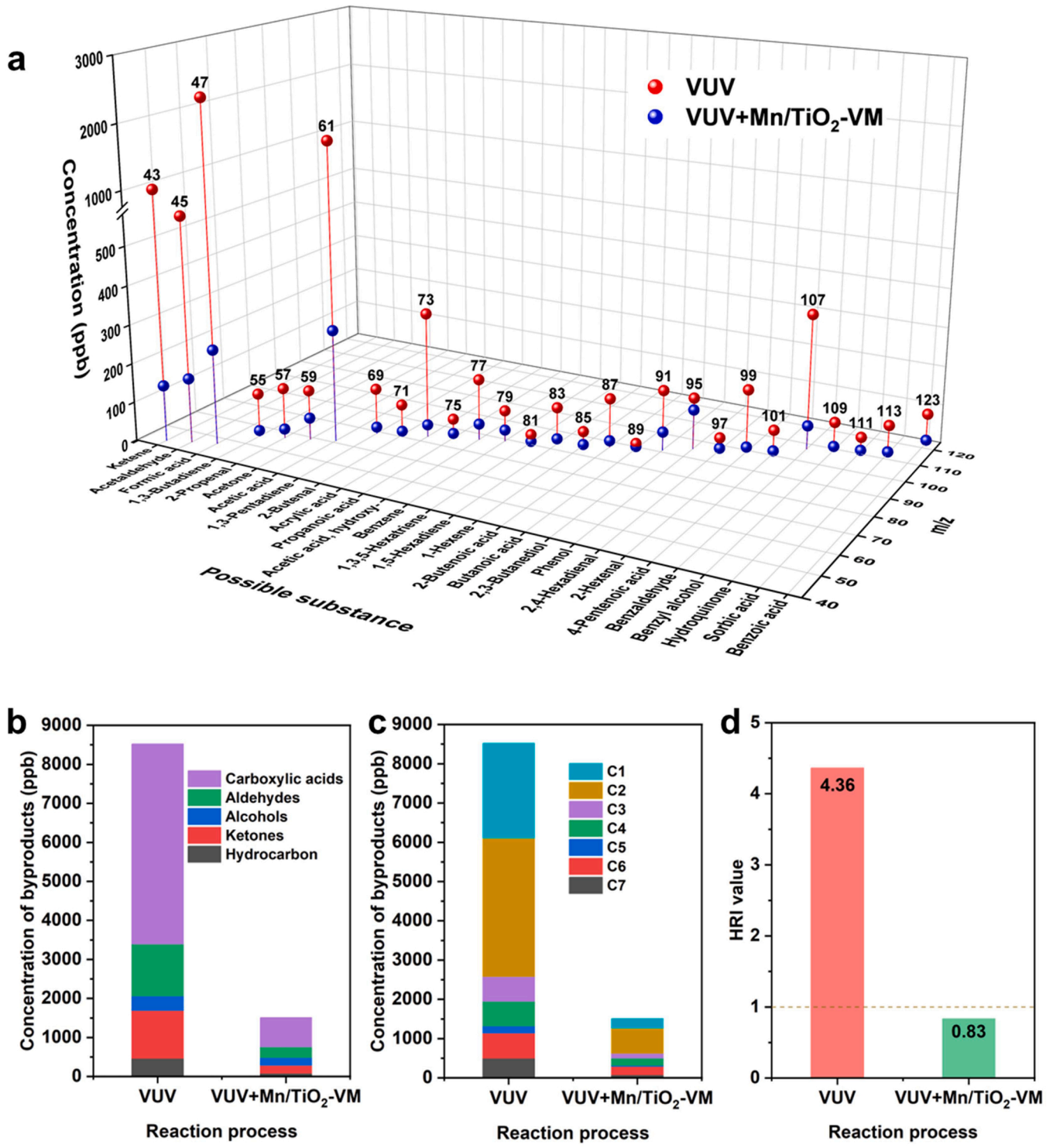

Fig. 7. Concentrations of organic byproducts based on PTR-TOF-MS results (the structural formulas of inferred byproducts with different *m/z* are shown in Table S7) (a). Total concentration of various types of organics byproducts (b). Total concentration of organics byproducts with various C amount (e.g., C7 represents the total amount of organics containing 7 carbon atoms) (c). Health related index (HRI) of byproducts during toluene degradation in the VUV photolysis and VUV catalytic oxidation systems (d).

interface, time-resolved in situ DRIFTS experiments were performed for VUV catalytic toluene oxidation over TiO_2 and Mn/TiO_2-VM. For the first 30 min of toluene adsorption in dark, the characteristic peaks of toluene adsorption could be observed on both TiO_2 and Mn/TiO_2-VM (Figs. 6a, b, S16a and Table S5) [48]. The absorption bands of C–OH and C═O groups were observed due to the formation of benzyl alcohol and benzaldehyde intermediates from toluene oxidation by the surface energy of catalysts [48,49]. However, more peaks were found on the Mn/TiO_2-VM surface, proving that multiple active sites could pre-oxidize toluene and generate more intermediates on the catalyst surface via strong chemical adsorption with π bonds of toluene. After the absorption process of 30 min, the VUV lamp was turned on (Figs. 6c, d, S16b and Table S6). It can be found that the peaks intensities of C═O (1651, 1533 and 1225 cm^{-1}) and methyl group (–CH_3, 1428, 1413,

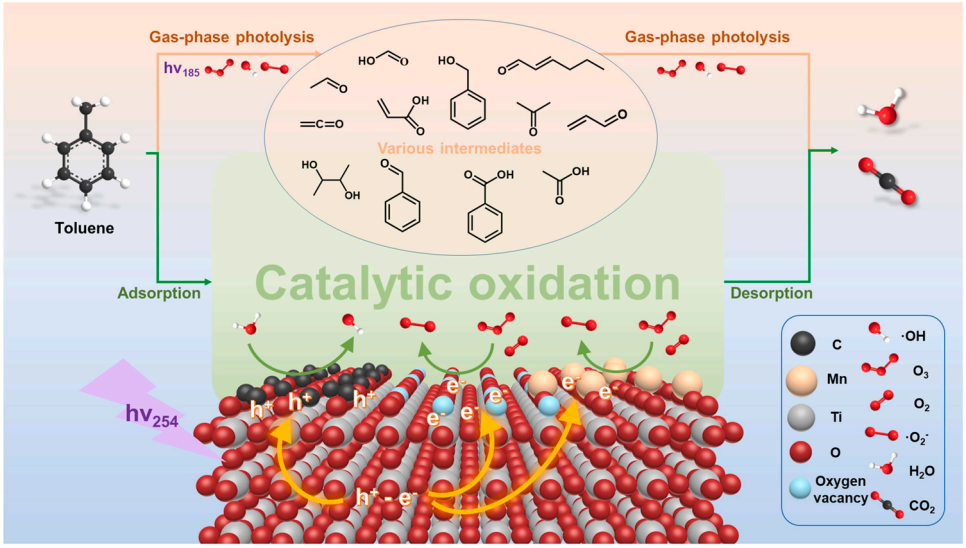

Scheme 1. Toluene degradation mechanism over Mn/TiO_2-VM in VUV catalytic oxidation.

1336 and 1314 cm^{-1}) were increased on both TiO_2 and Mn/TiO_2-VM surface. In particular, Mn/TiO_2-VM showed much more and stronger peaks of functional groups than TiO_2, indicating more efficient catalytic oxidation of toluene to generate more intermediates. Also, more efficient and deeper oxidation at catalyst interface can result in fewer intermediates being discharged to outlet in the gas-phase. The results were in well consistent with the plentiful ROS for toluene oxidation over Mn/TiO_2-VM. New peaks of –COOH at 1587 and 1360 cm^{-1}, which were properly originated from the accumulation of carboxylate (e.g., benzoic acid, acetic acid, formic acid), were apparently observed over TiO_2 during VUV catalytic oxidation while such peaks did not appear over Mn/TiO_2-VM. Previous studies indicated that the substances of carboxylic acids readily adhere to the surface of the catalysts, which can block the active sites and result in catalytic deactivation [48].

The gaseous byproducts from VUV photolysis and VUV catalytic oxidation of toluene were collected and analyzed by PTR-TOF-MS, and 28 organic byproducts were detected from toluene degradation (Fig. 7a and Table S7). Compared with VUV photolysis alone, the addition of Mn/TiO_2-VM significantly reduced the byproducts of ketene, acetaldehyde, formic acid, acetic acid and benzaldehyde, respectively, which could be easily adsorbed and further catalytically oxidized on Mn/TiO_2-VM surface. Fig. 7b and c showed that the concentration of byproducts was reduced by 82% in the presence of Mn/TiO_2-VM when compared with VUV photolysis alone. Especially, the short carbon chain byproducts of aldehydes and carboxylic acids were dramatically decreased. This result was well consistent with high toluene mineralization rate over Mn/TiO_2-VM. The health related index (HRI) values of outlet gas in different systems were calculated (Eqs. (S5)-(S6) in Text S9). It was found that the HRI value reached 4.36 in VUV photolysis alone (Fig. 7d) because of the existence of highly toxic byproducts such as high concentration of ketene, benzene and 2-propenal. However, the HRI value dropped to only 0.83 in the VUV catalytic oxidation system, which was within the exposure limit to human body and environment [50], indicating that the risk of byproducts was greatly decreased in the presence of catalytic oxidation. Therefore, compared with VUV photolysis alone, VUV catalytic oxidation can significantly improve toluene degradation performance as well as mitigate both various byproducts and environmental risk, which presents a novel, efficient and environmental-friendly process for VOCs removal.

Based on the above results, the deep oxidation mechanism of toluene in VUV catalytic oxidation with Mn/TiO_2-VM is proposed in Scheme 1. When toluene is introduced into the VUV catalytic oxidation system, the

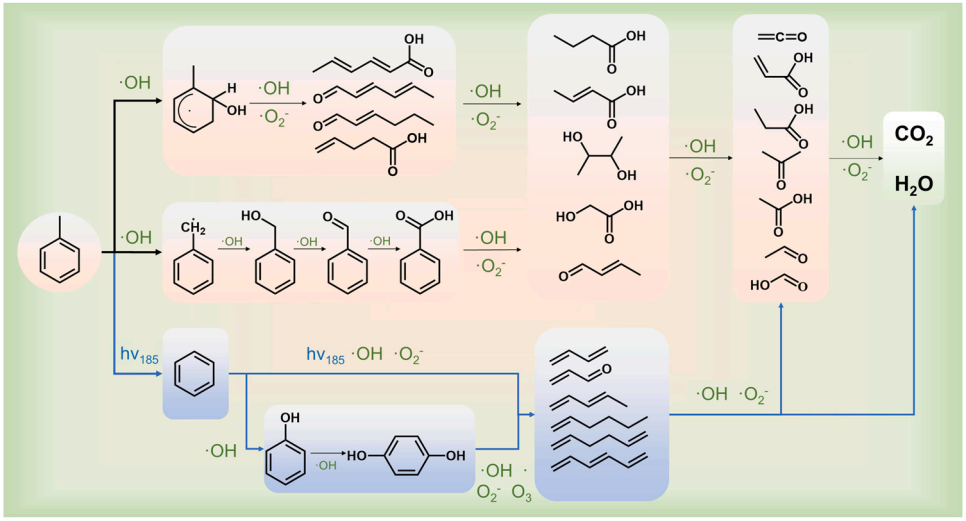

Scheme 2. Degradation pathways of toluene in the VUV catalytic oxidation system.

generated ·OH, $\cdot O_2^-$ and O_3 in the gas-phase environment (Eqs. 1–6) will oxidize partial toluene through gas-phase photolysis into various intermediates (Table S7) and a small fraction of CO_2 and H_2O. Partial toluene and intermediates in the gas-phase adhere to the surface of the Mn/TiO_2-VM catalyst through adsorption. Under the excitation of $h\nu_{254}$, Mn/TiO_2-VM generates photogenerated carriers (Eq. (7)), and h^+ will transfer to C site and e^- will transfer to O_v and Mn since the potential differences. H_2O actively reacts with h^+ on the C to form ·OH (Eq. (8)) while O_2 and O_3 react with e^- to effectively form $\cdot O_2^-$ on O_v and Mn (Eqs. (9) and (10)) at the catalyst interface, and e^- from photocatalysis promote O_3 catalysis and maintain the stability of Mn sites on the catalyst surface (Eqs. (11)–(13)). Additionally, O_v itself can also generate $\cdot O_2^-$ when adsorbing O_3 (Eqs. (14) and (15)). The ROS (·OH and $\cdot O_2^-$) generated at the catalyst interface will oxidize toluene and 28 byproducts into a large amount of CO_2 and H_2O for catalytic oxidation. It is precisely due to the catalytic oxidation reaction caused by bifunctional Mn/TiO_2-VM that $h\nu_{254}$ and O_3 in the VUV system are further utilized to achieve high mineralization rate of pollutants. Moreover, toluene degradation pathways in the VUV catalytic oxidation system are proposed based on the PTR-TOF-MS results and previous studies (Scheme 2) [22,51]. Most of the degradation pathways are carried out through the reaction of ROS, proving that catalytic oxidation can accelerate the process of these path reactions and mineralization of toluene and byproducts.

3.3.1. *Reactions at the catalyst interface under the VUV system*

$$h\nu_{254} + \text{catalyst} \rightarrow \text{catalyst}\ (h^+ + e^-) \quad (7)$$

$$h^+ + H_2O \rightarrow \cdot OH + H^+ \quad (8)$$

$$O_2 + e^- \rightarrow \cdot O_2^- \quad (9)$$

$$O_3 + e^- \rightarrow \cdot O_2^- + O(^1D) \quad (10)$$

$$Mn^{n+} + O_3 \rightarrow O^{2-} + Mn^{(n+2)+} + O_2 \quad (11)$$

$$O_3 + O^{2-} + Mn^{(n+2)+} \rightarrow Mn^{(n+2)+} + O_2 + O_2^{2-} \quad (12)$$

$$O_2^{2-} + e^- + Mn^{(n+2)+} \rightarrow \cdot O_2^- + Mn^{n+} \quad (13)$$

$$O_v + O_3 \rightarrow \cdot O^- + O_2 \quad (14)$$

$$\cdot O^- + O_3 \rightarrow \cdot O_2^- + O_2 \quad (15)$$

4. Conclusions

In this study, the bifunctional Mn/TiO_2-VM catalyst is originally developed for VUV catalytic oxidation of VOCs. Catalytic oxidation of Mn/TiO_2-VM well cooperated with gas-phase photolysis to achieve effective toluene oxidation via efficient utilization of $h\nu_{254}$ and O_3 byproduct from photolysis. Besides of superior toluene mineralization and energy utilization, the emissions of organic and O_3 byproducts as well as the consequential environmental risk were significantly reduced in the VUV catalytic oxidation system, demonstrating its high efficiency, energy saving and environment-friendliness. This study dramatically promotes the understanding of the VUV-based catalytic technology in the removal of low-concentration VOCs and provides key theoretical support for industrial application. It can be foreseen that VUV catalytic oxidation system can also be applied to effectively remove other VOCs and odor substances besides of aromatic VOCs. Additionally, the VUV lamp and raw materials for Mn/TiO_2-VM are commercially available and low-cost, so the technology is expected to be industrially applied for waste gas treatment in a large scale and greatly mitigate air pollution.

CRediT authorship contribution statement

Shengjun Ye: Conceptualization, Methodology, Investigation, Writing – original draft, Writing – review & editing, Data curation. **Xiaoying Lian**: Investigation, Methodology. **Biyuan Liu**: Formal analysis, Methodology. **Haibao Huang**: Conceptualization, Writing – review & editing, Supervision, Funding acquisition. **Boge Zhang**: Formal analysis, Methodology. **Zhuofeng Hu**: Resources, Writing – review & editing. **Xianliang Fu**: Writing – review & editing. **Guangqin Li**: Writing – review & editing. **Zhenpan Zhang**: Investigation.

Declaration of Competing Interest

The authors declare that they have no known competing financial interests or personal relationships that could have appeared to influence the work reported in this paper.

Data availability

No data was used for the research described in the article.

Acknowledgments

This work was supported by National Natural Science Foundation of China (22076224 and 22276223) and Program for Guangdong Introducing Innovative and Entrepreneurial Teams (2017ZT07C069).

Appendix A. Supporting information

Supplementary data associated with this article can be found in the online version at doi:10.1016/j.apcatb.2023.122802.

References

[1] K. Li, D.J. Jacob, H. Liao, J. Zhu, V. Shah, L. Shen, K.H. Bates, Q. Zhang, S. Zhai, A two-pollutant strategy for improving ozone and particulate air quality in China, Nat. Geosci. 12 (2019) 906–910.
[2] L. Zhu, D. Shen, K.H. Luo, A critical review on VOCs adsorption by different porous materials: Species, mechanisms and modification methods, J. Hazard Mater. 389 (2020), 122102.
[3] W. Wei, S. Wang, J. Hao, S. Cheng, Projection of anthropogenic volatile organic compounds (VOCs) emissions in China for the period 2010–2020, Atmos. Environ. 45 (2011) 6863–6871.
[4] C.J. Davidson, J.H. Hannigan, S.E. Bowen, Effects of inhaled combined Benzene, Toluene, Ethylbenzene, and Xylenes (BTEX): Toward an environmental exposure model, Environ. Toxicol. Pharmacol. 81 (2021).
[5] B. Huang, C. Lei, C. Wei, G. Zeng, Chlorinated volatile organic compounds (Cl-VOCs) in environment — sources, potential human health impacts, and current remediation technologies, Environ. Int. 71 (2014) 118–138.
[6] P. Wu, X. Jin, Y. Qiu, D. Ye, Recent Progress of Thermocatalytic and Photo/Thermocatalytic Oxidation for VOCs Purification over Manganese-based Oxide Catalysts, Environ. Sci. Technol. 55 (2021) 4268–4286.
[7] X.L. Weng, P.F. Sun, Y. Long, Q.J. Meng, Z.B. Wu, Catalytic Oxidation of Chlorobenzene over Mn_xCe_1-xO_2/HZSM-5 Catalysts: A Study with Practical Implications, Environ. Sci. Technol. 51 (2017) 8057–8066.
[8] A. Luengas, A. Barona, C. Hort, G. Gallastegui, V. Platel, A. Elias, A review of indoor air treatment technologies, Rev. Environ. Sci. Bio/Technol. 14 (2015) 499–522.
[9] X. Hao, X. Xiafan, C. Liubiao, G. Jia, W. Junjie, A novel cryogenic condensation system based on heat-driven refrigerator without power input for volatile organic compounds recovery, Energy Convers. Manag. 238 (2021), 114157.
[10] S.J. Li, X.Q. Dang, X. Yu, G. Abbas, Q. Zhang, L. Cao, The application of dielectric barrier discharge non-thermal plasma in VOCs abatement: A review, Chem. Eng. J. 388 (2020).
[11] J.Y. Li, R.M. Chen, W. Cui, X. Dong, H. Wang, K.H. Kim, Y.H. Chu, J.P. Sheng, Y. J. Sun, F. Dong, Synergistic Photocatalytic Decomposition of a Volatile Organic Compound Mixture: High Efficiency, Reaction Mechanism, and Long-Term Stability, ACS Catal. 10 (2020) 7230–7239.
[12] A. Talaiekhozani, S. Rezania, K.-H. Kim, R. Sanaye, A.M. Amani, Recent advances in photocatalytic removal of organic and inorganic pollutants in air, J. Clean. Prod. 278 (2021).

[13] B. Liu, J. Ji, B. Zhang, W. Huang, Y. Gan, D.Y.C. Leung, H. Huang, Catalytic ozonation of VOCs at low temperature: A comprehensive review, J. Hazard. Mater. 422 (2022), 126847.

[14] M. Wu, H. Huang, D.Y.C. Leung, A review of volatile organic compounds (VOCs) degradation by vacuum ultraviolet (VUV) catalytic oxidation, J. Environ. Manag. 307 (2022), 114559.

[15] Y. Liu, Q. Wang, J. Pan, Novel Process of Simultaneous Removal of Nitric Oxide and Sulfur Dioxide Using a Vacuum Ultraviolet (VUV)-Activated $O_2/H_2O/H_2O_2$ System in A Wet VUV-Spraying Reactor, Environ. Sci. Technol. 50 (2016) 12966–12975.

[16] T. Xu, H. Zheng, P. Zhang, Performance of an innovative VUV-PCO purifier with nanoporous TiO_2 film for simultaneous elimination of VOCs and by-product ozone in indoor air, Build. Environ. 142 (2018) 379–387.

[17] Q. Zhang, L. Wang, B. Chen, Y. Chen, J. Ma, Understanding and modeling the formation and transformation of hydrogen peroxide in water irradiated by 254 nm ultraviolet (UV) and 185 nm vacuum UV (VUV): Effects of pH and oxygen, Chemosphere 244 (2020), 125483.

[18] Y. Shu, J. Ji, Y. Xu, J. Deng, H. Huang, M. He, D.Y.C. Leung, M. Wu, S. Liu, S. Liu, G. Liu, R. Xie, Q. Feng, Y. Zhan, R. Fang, X. Ye, Promotional role of Mn doping on catalytic oxidation of VOCs over mesoporous TiO_2 under vacuum ultraviolet (VUV) irradiation, Appl. Catal. B: Environ. 220 (2018) 78–87.

[19] X. Sun, C. Li, B. Yu, J. Wang, W. Wang, Removal of gaseous volatile organic compounds via vacuum ultraviolet photodegradation: Review and prospect, J. Environ. Sci. 125 (2023) 427–442.

[20] Z. Shayegan, C.-S. Lee, F. Haghighat, TiO_2 photocatalyst for removal of volatile organic compounds in gas phase – A review, Chem. Eng. J. 334 (2018) 2408–2439.

[21] Y. Zhang, M. Wu, Y.H. Kwok, Y. Wang, W. Zhao, X. Zhao, H. Huang, D.Y.C. Leung, In-situ synthesis of heterojunction TiO_2/MnO_2 nanostructure with excellent performance in vacuum ultraviolet photocatalytic oxidation of toluene, Appl. Catal. B: Environ. 259 (2019).

[22] S. Liang, Y. Shu, K. Li, J. Ji, H. Huang, J. Deng, D.Y.C. Leung, M. Wu, Y. Zhang, Mechanistic insights into toluene degradation under VUV irradiation coupled with photocatalytic oxidation, J. Hazard. Mater. 399 (2020), 122967.

[23] Y. Zhang, M. Wu, Y. Wang, Y.H. Kwok, W. Pan, W. Szeto, H. Huang, D.Y.C. Leung, Fluorinated TiO_2 coupling with α-MnO_2 nanowires supported on different substrates for photocatalytic VOCs abatement under vacuum ultraviolet irradiation, Appl. Catal. B: Environ. 280 (2021).

[24] J. Chen, Z. He, Y. Ji, G. Li, T. An, W. Choi, OH radicals determined photocatalytic degradation mechanisms of gaseous styrene in TiO_2 system under 254 nm versus 185 nm irradiation: Combined experimental and theoretical studies, Appl. Catal. B: Environ. 257 (2019).

[25] Y. Long, Y. Su, Y. Xue, Z. Wu, X. Weng, V_2O_5-WO_3/TiO_2 Catalyst for Efficient Synergistic Control of NO_x and Chlorinated Organics: Insights into the Arsenic Effect, Environ. Sci. Technol. 55 (2021) 9317–9325.

[26] R. Zhang, C. Song, M. Kou, P. Yin, X. Jin, L. Wang, Y. Deng, B. Wang, D. Xia, P. K. Wong, L. Ye, Sterilization of Escherichia coli by Photothermal Synergy of WO_{3-x}/C Nanosheet under Infrared Light Irradiation, Environ. Sci. Technol. 54 (2020) 3691–3701.

[27] Y. Fang, H. Li, Q. Zhang, C. Wang, J. Xu, H. Shen, J. Yang, C. Pan, Y. Zhu, Z. Luo, Y. Guo, Oxygen vacancy-governed opposite catalytic performance for C_3H_6 and C_3H_8 combustion: the effect of the Pt electronic structure and chemisorbed oxygen species, Environ. Sci. Technol. 56 (2022) 3245–3257.

[28] Y. Wang, Y. Zhang, X. zhu, Y. Liu, Z. Wu, Fluorine-induced oxygen vacancies on TiO_2 nanosheets for photocatalytic indoor VOCs degradation, Appl. Catal. B: Environ. 316 (2022), 121610.

[29] J. Safaei, H. Ullah, N.A. Mohamed, M.F. Mohamad Noh, M.F. Soh, A.A. Tahir, N. Ahmad Ludin, M.A. Ibrahim, W.N.R. Wan Isahak, M.A. Mat, Teridi, Enhanced photoelectrochemical performance of Z-scheme g-$C_3N_4/BiVO_4$ photocatalyst, Appl. Catal. B: Environ. 234 (2018) 296–310.

[30] J. Huang, L. Dou, J. Li, J. Zhong, M. Li, T. Wang, Excellent visible light responsive photocatalytic behavior of N-doped TiO_2 toward decontamination of organic pollutants, J. Hazard Mater. 403 (2021), 123857.

[31] L. Zhang, L. Shi, L. Huang, J. Zhang, R. Gao, D. Zhang, Rational Design of High-Performance $DeNO_x$ Catalysts Based on Mn_xCo_3–xO_4 Nanocages Derived from Metal–Organic Frameworks, ACS, Catalysis 4 (2014) 1753–1763.

[32] J. Ji, X. Lu, C. Chen, M. He, H. Huang, Potassium-modulated δ-MnO_2 as robust catalysts for formaldehyde oxidation at room temperature, Appl. Catal. B: Environ. 260 (2020).

[33] X. Yu, M. Shi, Y. Fan, L. Yang, J. Zhang, W. Liu, W. Dai, S. Zhang, L. Zhou, X. Luo, S. Luo, Activation or passivation: Influence of halogen dopant (F, Cl, Br) on photothermal activity of Mn_2O_3 in degrading toluene, Appl. Catal. B: Environ. 309 (2022).

[34] H. Shang, M. Li, H. Li, S. Huang, C. Mao, Z. Ai, L. Zhang, Oxygen vacancies promoted the selective photocatalytic removal of NO with blue TiO_2 via simultaneous molecular oxygen activation and photogenerated hole annihilation, Environ. Sci. Technol. 53 (2019) 6444–6453.

[35] A. León, P. Reuquen, C. Garín, R. Segura, P. Vargas, P. Zapata, P. Orihuela, FTIR and Raman Characterization of TiO_2 Nanoparticles Coated with Polyethylene Glycol as Carrier for 2-Methoxyestradiol, Appl. Sci. 7 (2017).

[36] N. Feng, H. Lin, H. Song, L. Yang, D. Tang, F. Deng, J. Ye, Efficient and selective photocatalytic CH_4 conversion to CH_3OH with O_2 by controlling overoxidation on TiO_2, Nat. Commun. 12 (2021) 4652.

[37] Z. Mengting, T.A. Kurniawan, R. Avtar, M.H.D. Othman, T. Ouyang, H. Yujia, Z. Xueting, T. Setiadi, I. Iswanto, Applicability of TiO_2(B) nanosheets@hydrochar composites for adsorption of tetracycline (TC) from contaminated water, J. Hazard. Mater. 405 (2021).

[38] B. Liu, B. Zhang, J. Ji, K. Li, J. Cao, Q. Feng, H. Huang, Effective regulation of surface bridging hydroxyls on TiO_2 for superior photocatalytic activity via ozone treatment, Appl. Catal. B-Environ. 304 (2022), 120952.

[39] S.-T. Xiao, S.-M. Wu, Y. Dong, J.-W. Liu, L.-Y. Wang, L. Wu, Y.-X. Zhang, G. Tian, C. Janiak, M. Shalom, Y.-T. Wang, Y.-Z. Li, R.-K. Jia, D.W. Bahnemann, X.-Y. Yang, Rich surface hydroxyl design for nanostructured TiO_2 and its hole-trapping effect, Chem. Eng. J. 400 (2020).

[40] L.H. Chen, E.Priatna Aripin, N. Busaeri, R. Priyadi, I.N. Sudiana, I.M. Joni, S. Sabchevski, Y. Kondo, Investigation on the Particle Growth of Rutile TiO_2 Suppressed by Manganese, MATEC Web Conf. 221 (2018).

[41] S. Eaimsumang, P. Prataksanon, S. Pongstabodee, A. Luengnaruemitchai, Effect of acid on the crystalline phase of TiO_2 prepared by hydrothermal treatment and its application in the oxidative steam reforming of methanol, Res. Chem. Intermed. 46 (2019) 1235–1254.

[42] W. Zhang, G. Innocenti, M. Ferbinteanu, E.V. Ramos-Fernandez, A. Sepulveda-Escribano, H. Wu, F. Cavani, G. Rothenberg, N.R. Shiju, Understanding the oxidative dehydrogenation of ethyl lactate to ethyl pyruvate over vanadia/titania, Catal. Sci. Technol. 8 (2018) 3737–3747.

[43] C. Xu, Y. Pan, G. Wan, H. Liu, L. Wang, H. Zhou, S.H. Yu, H.L. Jiang, Turning on visible-light photocatalytic C-H oxidation over metal-organic frameworks by introducing metal-to-cluster charge transfer, J. Am. Chem. Soc. 141 (2019) 19110–19117.

[44] B. Baral, K.H. Reddy, K.M. Parida, Construction of M-$BiVO_4$/T-$BiVO_4$ isotype heterojunction for enhanced photocatalytic degradation of Norfloxacine and Oxygen evolution reaction, J. Colloid Interface Sci. 554 (2019) 278–295.

[45] H. Shen, M. Lin, L. Wang, Z. Huang, X. Wu, X. Jiang, Q. Li, C.L. Chen, J. Zhao, G. Jing, C.S. Yuan, Experimental and theoretical investigation of the enhancement of the photo-oxidation of Hg_0 by CeO_2-modified morphology-controlled anatase TiO_2, J. Hazard Mater. 406 (2021), 124535.

[46] S. Ye, Y. Xu, L. Huang, W. Lai, L. Deng, Z. Lin, H. Peng, X. Zhou, G. Xie, MWCNT/$BiVO_4$ photocatalyst for inactivation performance and mechanism of *Shigella flexneri HL*, antibiotic-resistant pathogen, Chem. Eng. J. 424 (2021).

[47] X. Cao, Z. Chen, R. Lin, W.-C. Cheong, S. Liu, J. Zhang, Q. Peng, C. Chen, T. Han, X. Tong, Y. Wang, R. Shen, W. Zhu, D. Wang, Y. Li, A photochromic composite with enhanced carrier separation for the photocatalytic activation of benzylic C–H bonds in toluene, Nature, Catalysis 1 (2018) 704–710.

[48] H. Wang, Xa Dong, W. Cui, J. Li, Y. Sun, Y. Zhou, H. Huang, Y. Zhang, F. Dong, High-surface energy enables efficient and stable photocatalytic toluene degradationviathe suppression of intermediate byproducts, Catal. Sci. Technol. 9 (2019) 2952–2959.

[49] Z. Su, W. Si, H. Liu, S. Xiong, X. Chu, W. Yang, Y. Peng, J. Chen, X. Cao, J. Li, Boosting the Catalytic Performance of CeO_2 in Toluene Combustion via the Ce-Ce Homogeneous Interface, Environ. Sci. Technol. 55 (2021) 12630–12639.

[50] J. Mo, Y. Zhang, Q. Xu, Y. Zhu, J.J. Lamson, R. Zhao, Determination and risk assessment of by-products resulting from photocatalytic oxidation of toluene, Appl. Catal. B: Environ. 89 (2009) 570–576.

[51] Y. Shu, M. He, J. Ji, H. Huang, S. Liu, D.Y.C. Leung, Synergetic degradation of VOCs by vacuum ultraviolet photolysis and catalytic ozonation over Mn-xCe/ZSM-5, J. Hazard Mater. 364 (2019) 770–779.